analytical chemistry

Article

Cite This: *Anal. Chem.* 2019, 91, 11138−11145

pubs.acs.org/ac

Measurements of Immersion Freezing and Heterogeneous Chemistry of Atmospherically Relevant Single Particles with Micro-Raman Spectroscopy

Liora E. Mael,[†] Heidi Busse,[†] and Vicki H. Grassian*[,†,‡]

[†]Department of Chemistry and Biochemistry and [‡]Department of Nanoengineering and Scripps Institution of Oceanography, University of California−San Diego, La Jolla, California 92037, United States

Supporting Information

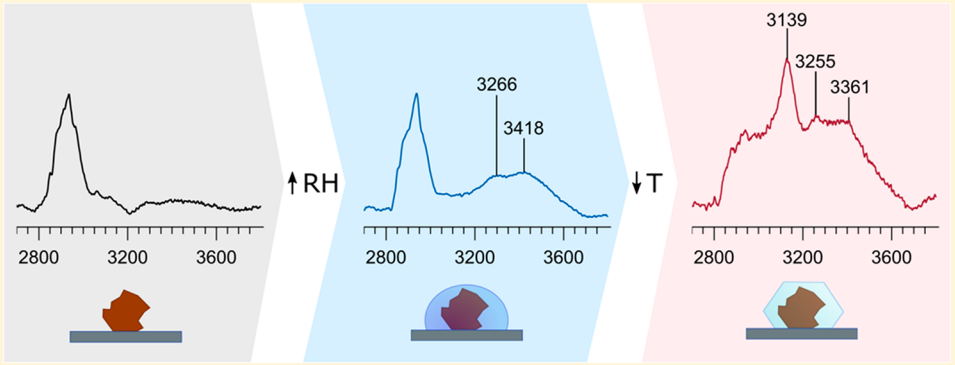

ABSTRACT: In the atmosphere, there are several different trajectories by which particles can nucleate ice; two of the major pathways are deposition and immersion freezing. Single particle depositional freezing has been widely studied with spectroscopic methods while immersion freezing has been predominantly studied either for particles within bulk aqueous solutions or using optical imaging of single particles. Of the few existing spectroscopic methods that monitor immersion freezing, there are limited opportunities for investigating the impact of heterogeneous chemistry on freezing. Herein, we describe a method that couples a confocal Raman spectrometer with an environmental cell to investigate single particle immersion freezing along with the capability to investigate in situ the impact of heterogeneous reactions with ozone and other trace gases on ice nucleation. This system, which has been rigorously calibrated (temperature and relative humidity) across a large dynamic range, is used to investigate low temperature water uptake and heterogeneous ice nucleation of atmospherically relevant single particles deposited on a substrate. The use of Raman spectroscopy provides important insights into the phase state and chemical composition of ice nuclei and, thus, insights into cloud formation.

Ice nucleating particles (INPs) play an important role in the formation of ice and mixed-phase clouds and therefore the Earth's hydrological cycle and global radiation budget,[1,2] all of which are essential for parameterizing climate models.[3] Ice clouds are predominantly composed of ice crystals, while mixed-phase clouds are comprised of both supercooled droplets and ice crystals and either found in colder regions of the atmosphere or extend to a higher altitude.[1] In addition to directly effecting albedo by deflecting incoming solar radiation or absorbing outgoing terrestrial radiation, it has been found that precipitation formation is more efficient in the presence of ice than in warmer clouds.[4] Changes in ice nucleation behavior will directly impact the formation of ice and mixed-phase clouds, which in turn effect precipitation, cloud cover, and optical depth.[1,5,6] Due to this complexity, the aerosol component in aerosol−cloud interactions remains one of the largest uncertainties in climate models.[7] Many of these uncertainties are due to the limited understanding of the physical and chemical principles that direct ice nucleation[8,9] and, therefore, ice cloud formation.

Broadly, ice can form in the Earth's atmosphere via two mechanisms: homogeneous and heterogeneous ice nucleation. Homogeneous ice nucleation occurs when a water droplet is supercooled below −35 °C and freezes in the absence of any foreign perturbation.[10] Heterogeneous ice nucleation occurs at warmer temperatures when ice formation is catalyzed by the presence of INPs.[10] Field studies have identified heterogeneous ice nucleation as the dominant formation mechanism in both ice and mixed-phase cloud formation.[5,11] INPs are rare in the atmosphere, estimated to be 1 in 10^5 to 10^6 particles,[12] which has led to a poor understanding of both their identity and the mechanism by which they nucleate ice.

Received: April 14, 2019
Accepted: August 2, 2019
Published: August 2, 2019

DOI: 10.1021/acs.analchem.9b01819
Anal. Chem. 2019, 91, 11138−11145

Two major pathways for heterogeneous ice formation are deposition and immersion freezing[13] as illustrated in Figure 1.

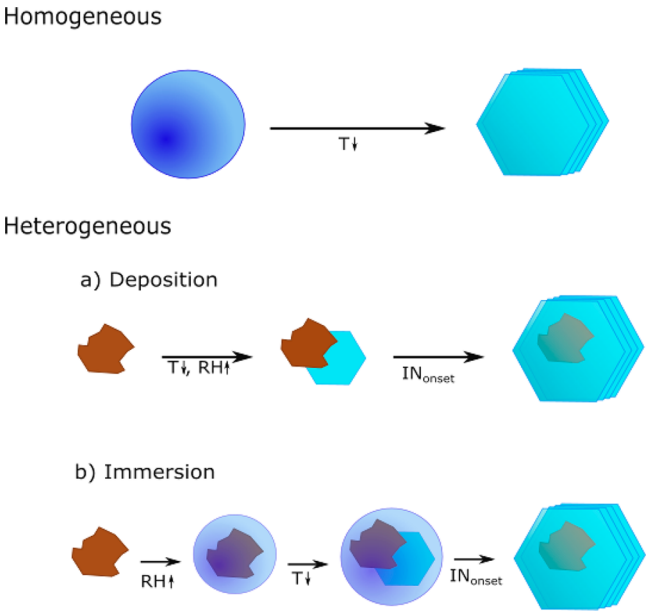

Figure 1. Comparison of homogeneous and (a) deposition and (b) immersion heterogeneous freezing.

Deposition freezing occurs by a decrease in temperature followed by an increase in humidity. Water vapor then adsorbs onto a solid surface, which initiates nucleation.[14,15] Immersion freezing occurs when the relative humidity (RH) is first increased, leading to condensed water, followed by a decrease in temperature, leading to the formation of a supercooled droplet and then ice. Many single particle INP studies focus on deposition freezing,[16−20] which is important in ice phase cloud formation,[11] but limits further understanding of ice nucleation processes and global cloud formation. Immersion freezing has been singled out as important for mixed-phase cloud formation, where INPs are expected to form droplets prior to freezing.[21−24]

A comprehensive review of immersion freezing techniques was conducted in 2015 using illite NX as a standard by Hiranuma and co-workers.[25] This study compared a wide range of techniques, including those used in the field (Continuous Flow Diffusion Chamber, CFDC) and laboratory (Leipzig Aerosol Cloud Interaction Simulator, LAICS), single particle[16,26] and well plate (Ice Spectrometer, IS) measurements, as well as systems with (Frankfurt Ice Deposition Freezing Experiment, FRIDGE) and without (Electrodynamic Balance, EDB, acoustic droplet levitator) substrates. Many of these aforementioned techniques and several not included in the study[27−29] monitor ice nucleation optically, but lack in situ spectroscopic analysis with exposure to different environments. The use of spectroscopic probes can provide insights into the chemical composition of INPs and mechanisms of ice nucleation.[30,31] This is especially relevant for understanding the ice nucleation behavior of sea spray aerosol (SSA), where the chemical components which mediate ice nucleation remain poorly understood.[32]

Tolbert and co-workers as well as Knopf and co-workers have detailed a system that couples an environmental cell to a Raman spectrometer, which has predominantly been used to study deposition freezing[16,33−35] and, in some cases, immersion freezing.[25,36−38] However, the techniques developed focused on isolating the INP from its surrounding either by depositing the droplet and then sealing it in small chamber or by immersing the droplet in a layer of silicon oil. Both methods effectively maintain the conditions the droplet was deposited in, but limits in situ study of heterogeneous chemistry, and the effect this chemistry has on ice nucleation behavior.

Therefore, there exists a need to develop a single particle technique with heterogeneous chemistry abilities that measures immersion freezing with optical and spectral probes of SSA. To meet this need, we have coupled a micro-Raman spectrometer with an environmental cell to measure immersion freezing by cooling single particles composed of ice nucleation standards and marine relevant systems. This system has the unique capability to obtain in situ, real-time measurements of the composition and phase state of INPs with the option of flowing in reactive gases and facilitates the study of the kinetics and effects of heterogeneous chemistry on ice nucleation.

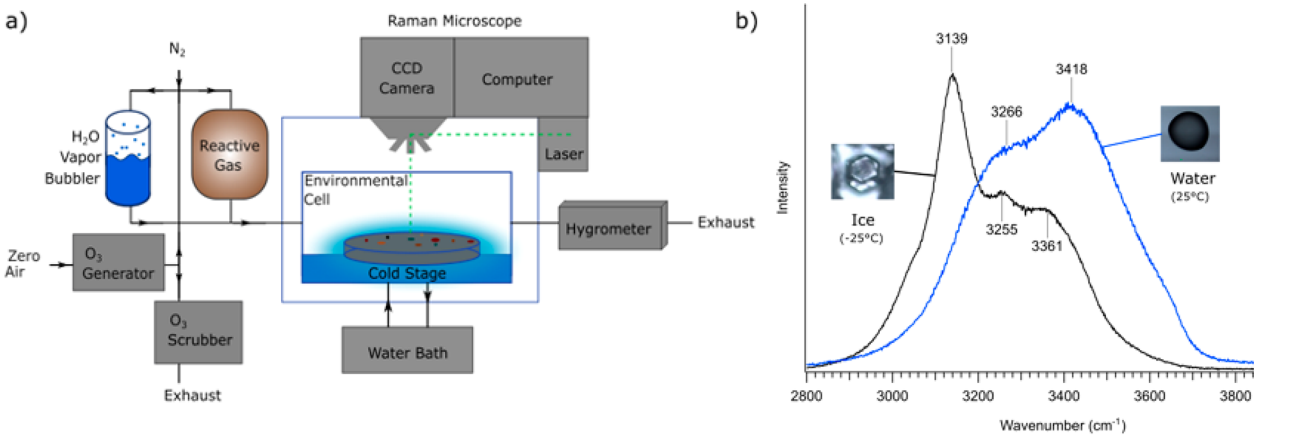

Figure 2. (a) Schematic of the Raman microscope coupled to an environmental cell for immersion freezing studies of substrate deposited aerosol particles. (b) Raman spectra and optical images of droplets of pure ice (black) and water (blue), at −25 and 25 °C, respectively. Relative humidity is controlled through mixing wet and dry air of varying ratios.

DOI: 10.1021/acs.analchem.9b01819
Anal. Chem. 2019, 91, 11138−11145

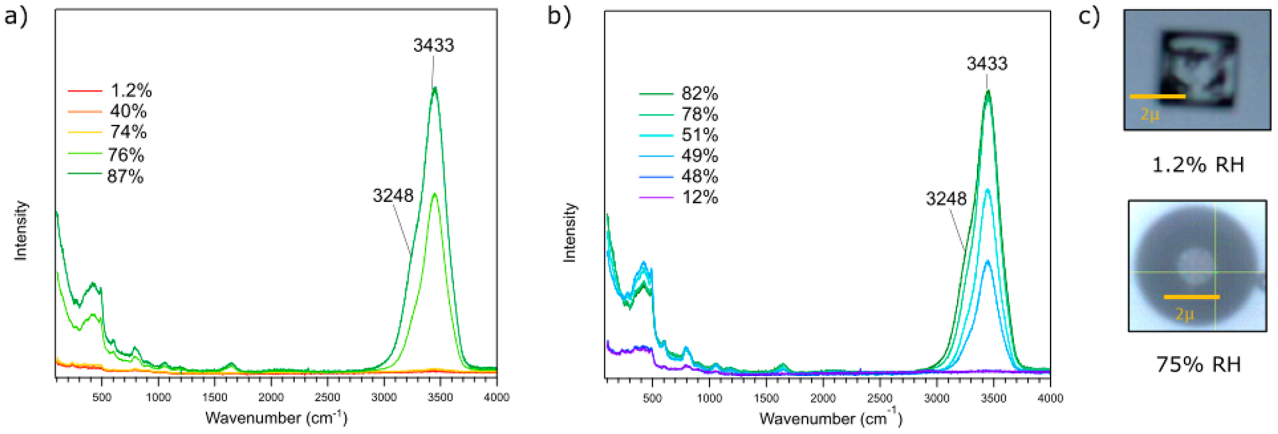

Figure 3. Raman spectra of deliquescence (a) and efflorescence (b) of a single particle of NaCl with (c) accompanying optical images of dry (1.2% RH) and wet (75% RH) NaCl particles.

EXPERIMENTAL METHODS

Instrumentation. Ice nucleation and water uptake measurements were preformed using a Raman microscope (Horiba, LabRamn HR Evolution) coupled to an environmental cell (Linkam, LTS 120), as shown in Figure 2. The spectrometer is fit with an optical microscope (Olympus BX41), a 100× super long working distance (SLWD) objective, and a 532 nm laser. The environmental cell has inlets for gases and an exhaust line connected to a hygrometer (Buck, CR-4) and a temperature controller (Linkam, T-95 PE), which allow for temperature and RH control. RH is controlled by sending N_2 through a bubbler of Milli-Q water and modulating the ratio of wet to dry N_2 flowing into the environmental cell. The ozone system is comprised of an ozone generator (Jelight Company Inc., Model No. 2000) and an ozone scrubber (Ozone Solutions, Inc.).

Source of Chemicals. Aqueous solutions were prepared with Milli-Q ultrapure water and commercially available compounds, including *Pseudomonas syringae* (Snomax), York Snow Inc.; kaolinite (KGa-1b), The Clay Mineral Society; montmorillonite (SAz-1), The Clay Mineral Society; illite NX (NX Nanopowder), Arginotec; lipase (from *Pseudomonas cepacia*), Sigma-Aldrich; lysozyme (from chicken egg white), Sigma-Aldrich; lipopolysaccharide (LPS, L4130, extracted from *E. coli* DIIILB4, purified by trichloroacetic acid extraction), Sigma-Aldrich; sodium chloride (NaCl), ≥99% Fischer Scientific; sodium nitrate ($NaNO_3$), ≥99% Sigma-Aldrich; sodium sulfate (Na_2SO_4), ≥99.0% Sigma-Aldrich; ammonium nitrate (NH_4NO_3), ≥98% Sigma-Aldrich; ammonium sulfate ($(NH_4)_2SO_4$), ≥99% Sigma-Aldrich; oleic acid, Fischer.

Sample Preparation and Data Collection of Single Particles. Samples were generated by atomizing aqueous solutions of the above compounds. Particles were passed through two silica diffusion driers (RH < 5%) and impacted on hydrophobically coated (RainX) quartz discs (Ted Pella, No. 16001-1). The discs were then placed inside the environmental cell where water uptake and ice nucleation were monitored on a particle-to-particle basis as well as with spectral maps to determine variability in phase and chemical composition. The cell has a working temperature range of −26.5 to 120.0 ± 0.4 °C and RH control from 1.3 to 99.0 ± 2.1%. A 532 nm laser and the 100× SLWD objective were used to probe particles between 1 and 4 μm in diameter. A total of 2−11 exposures of 3−45 seconds each were averaged to obtain each spectrum in the spectral range extending from 400 to 4000 cm^{-1}.

Ozone Exposure Experiments. To probe the impacts of oxidation on ice nucleation behavior, a sample was first deposited and placed in the environmental cell. Following this, the N_2 purge was replaced with ozone, and RH was set at 50 ± 2.1%. Once equilibrated, the system was reacted with ∼10 ppm of ozone for 1 hour, and subsequent ice nucleation experiments were conducted. The ozone concentration was measured using an ozone monitor (Ozone Solutions) before and after the environmental cell. These concentrations were approximately the same with a fluctuation of 5 ppb from the initial ozone introduction toward the end of the 1 hour time period indicating minimal loss of ozone to the walls of the environmental cell.

Calibration of Environmental Cell for Ice Nucleation Measurements. Water uptake measurements were done with several well-characterized inorganic model systems by varying the ratio of wet to dry flow into the environmental cell. Prior to each experiment, deposited samples were dried in the cell under N_2 for a 20 min calibration period. Following this were incremental increases in RH (from 0.3 through 85 to 95%) with 10 min equilibration periods in between. A Raman spectrum was collected following each incremental change in RH. Both visual and spectral observations confirmed deliquescence with an increase in particle size, the darkening of the droplet observed via optical microscopy, and the growth of the O−H stretching region between 3200 to 3800 cm^{-1}, as seen in Figure 3.

Once deliquescence occurred, the temperature and dew point measurements from the hygrometer were used to calculate the RH in the cell, adapted from Murphy and Koop[39] and shown in eqs 1−6:

$$\mathrm{RH} = \frac{p_{l\ \mathrm{or}\ i}}{p^{o}} \times 100 \tag{1}$$

$$p_l \approx \exp\left(54.842763 - \frac{6763.22}{T_d} - 4.210\ln[T_d] + 0.000367T_d + \tanh[0.0415\{T_d - 218.8\}]\left[53.878 - \frac{1331.22}{T_d} - 9.44523\ln(T_d) + 0.014025T_d\right]\right) \quad \text{for} \quad T_d \geq 273.15\ \mathrm{K} \tag{2}$$

DOI: 10.1021/acs.analchem.9b01819
Anal. Chem. 2019, 91, 11138−11145

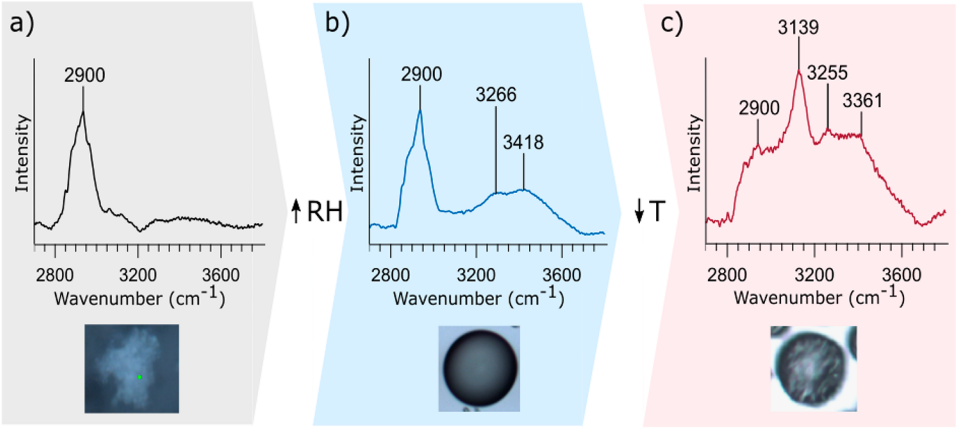

Figure 4. Schematic diagram showing the process of immersion freezing using micro-Raman spectroscopy: (a) shows a spectrum and an optical image of a dry particle; (b) a particle after deliquescence, where two new absorption bands are seen at 3266 and 3418 cm^{-1}, corresponding to liquid water; and (c) the same particle at lower temperature where ice freezes as seen by the vibrational bands at 3139, 3255, and 3361 cm^{-1}.

$$p_i = \exp\left(9.550426 - \frac{5723.265}{T_d} + 3.53068 \ln[T_d] - 0.00728332 T_d\right) \quad \text{for} \quad 110 < T_d < 273.15 \text{ K} \tag{3}$$

$$p^\circ_{EC} = p^\circ_{TR} \exp\left[-\frac{L_{l \text{ or } sl}}{R_v}\left(\frac{1}{T_{EC}} - \frac{1}{T_{TR}}\right)\right] \tag{4}$$

$$L_l = 1.91846 \times 10^6 \left[\frac{T_{EC}}{T_{EC} - 33.91}\right]^2 \quad \text{for } T_{EC} \geq 273.15 \text{ K} \tag{5}$$

$$L_{sl} = 56579 - 42.212 T_{EC} + \exp(0.1149[281.6 - T_{EC}]) \quad \text{for } 236 \leq T_c \leq 273.15 \text{ K} \tag{6}$$

where in eqs 1−6, p is the water vapor pressure either of a liquid water (l) when $T_d \geq 273.15$ K, where T_d is the dew point temperature, or ice (i) when $T_d < 273.15$ K, p° is the water saturation vapor pressure, subscripts EC and TR refer the value of the temperature and pressure in the environmental cell and at the triple point for water, respectively, L is the latent heat of vaporization for water either of a liquid (l) when $T_{EC} \geq 273.15$ K or a supercooled liquid (sl) when $T_{EC} < 273.15$ K, and R_v is the ideal gas constant.[39] Note that T_{EC} is the temperature in the environmental cell, but for the water uptake measurements made at ambient temperature, it is assumed that it is the same as the temperature of the hygrometer. The reverse process was followed for efflorescence. The comparison of experimental and literature deliquescence and efflorescence values for a range of salt compounds that include NaCl, $NaNO_3$, Na_2SO_4, NH_4NO_3, and $(NH_4)_2SO_4$ are given in the Supporting Information (Figure S1) and fall closely within the range of reported literature values.[40−43]

In addition to water uptake, ice nucleation measurements rely on accurate temperature measurements. A calibration of the environmental cell was done to account for any differences in the set temperature and the temperature of the substrate deposited particles in the cell.[44] Using the water uptake properties of NaCl, which have been shown to have a deliquescence relative humidity (DRH) of 75% over a broad range of temperatures,[45] a calibration curve was generated by back calculating the temperature[44,46] that the particles experienced at different set temperatures, rearranging eqs 1 and 4. New NaCl samples were prepared for each DRH measurement. The deliquescence protocol described above was followed, with the addition of a 20 min temperature calibration period following the initial drying. Spectra were collected to confirm deliquescence at each temperature and are shown in Supporting Information, Figure S2. Supporting Information, Figure S3 shows the correlation between the set temperatures and the actual temperature. There is good linearity through the range of set temperatures from −40 to 25 °C.

Immersion Ice Nucleation Experiments. In a typical immersion freezing experiment, a sample is placed in the environmental cell and deliquesced, as discussed above. The RH was typically increased further until the sample was completely immersed, and a spectrum confirmed water uptake. Once the RH had stabilized, the temperature in the cell was dropped (−4.1 °C/min) and the RH was modulated following the trajectories shown in Supporting Information, Figure S4, to maintain a constant RH. As the temperature decreased, spectra were collected continuously every one second, monitoring the 2800 to 3800 cm^{-1} range for changes in the O−H stretch, specifically the appearance of the distinct low frequency 3139 cm^{-1} peak, indicating ice formation, as shown in Figure 2. Additionally, this process can be monitored through the optical microscope video feed, looking for the appearance of optical interference indicating ice nucleation.

The water uptake and immersion freezing process for a single particle and the associated spectra are shown in Figure 4. With the optical microscope, visual monitoring allowed for the ice nucleation onset temperature to be recorded as the temperature where ice nucleation was first observed. The ice nucleation measurements are made on a substrate, and as such, once one particle nucleates, it can initiate nucleation when there is contact between particles. These measurements are distinct from other ice nucleation measurements done in individual wells, where one ice nucleation event does not affect another.

RESULTS AND DISCUSSION

The ice nucleation behavior of a variety of different atmospherically relevant particles including Snomax, kaolinite, montmorillonite, illite NX, lysozyme, lipase, and lipopolysaccharide (LPS) were measured using the environmental cell

DOI: 10.1021/acs.analchem.9b01819
Anal. Chem. 2019, 91, 11138−11145

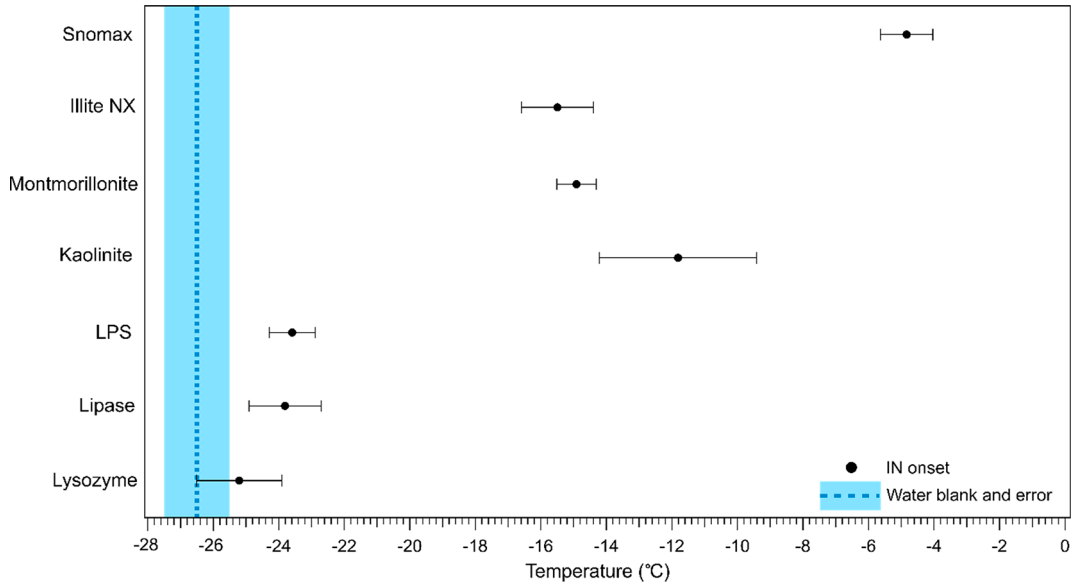

Figure 5. Ice nucleation onset temperatures for LPS, lipase, lysozyme, montmorillonite, kaolinite, Snomax, and illite NX. The blue dashed line is the freezing temperature of the water blank, and the shaded blue area indicates the uncertainty in the measurement, as determined by the upper and lower values experimentally measured.

coupled micro-Raman spectroscopy. Snomax, kaolinite, montmorillonite, and illite NX were chosen as standards; immersion freezing of these systems has been well characterized in the literature across a variety of different immersion ice nucleation systems.[47−53]

Snomax, a lysed strain of *Pseudomonas syringae*, is an excellent INP, initiating freezing as warm as −2 °C.[54] The ice nucleation behavior of Snomax has been attributed to a specific protein complex on the surface of the bacterial membrane that orders water molecules, which facilitates ice nucleation.[55] As already noted, Snomax was selected as a standard in this study because of its extensive characterization in the literature[48,56−61] and its warm freezing temperature. It was experimentally determined that the freezing of Snomax occurred at −4.8 ± 0.8 °C in this system.

Kaolinite, montmorillonite, and illite are common clay minerals that have been investigated and used as ice nucleation benchmark standards.[13,25,50] Illite NX is used in this study for consistency with Hiranuma et al.[25] There is a lot of variability in ice nucleation temperatures reported, and much of that can be attributed to the size dependence of their ice nucleation behavior.[62−66] We found these minerals to nucleate ice at −11.8 ± 2.4, −14.9 ± 0.6, and −15.5 ± 1.1 °C for kaolinite, montmorillonite, and illite NX, respectively, as shown in Figure 5. These values correlate with literature ice nucleation values for similarly sized particles on the order of 1 to 2 μm. Additionally, these minerals freeze ice in the middle of the temperature range investigated here.

In addition to measurement of these standards, the homogeneous freezing temperature of water was measured and is shown as the dashed blue line in Figure 5. Water droplets produced from Milli-Q ultrapure water freeze at −26.5 ± 0.9 °C, warmer than the homogeneous, atmospheric freezing temperature of −38 °C, but within the range reported in literature for laboratory studies.[36,67−69] Steps were taken to decrease the ice nucleation onset temperature of pure water, including minimizing sample exposure to ambient air, using Milli-Q ultrapure water, and altering the rate at which the temperature was changed. The current experimental parameters, as described in the Experimental Methods, have yielded the lowest freezing temperature of pure water. The freezing temperature does not affect the ice nucleation onset temperature of the standards, leading to the conclusion that any ice nucleation measurements warmer than the measured homogeneous freezing temperature of water are valid.

Overall, ice nucleation onset temperatures of Snomax, kaolinite, montmorillonite, and illite NX show good agreement with literature values (Table 1). This agreement between the current measurements and the literature values, which were collected using other methods, confirms the validity and viability of the current method. A small degree of variation in these measurements is due to experimental differences, including the size of particles and the time dependence of ice nucleation. However, values measured here all fall within the range of ice nucleation values reported in literature for comparably sized particles.

Table 1. Comparison of Experimental and Literature Ice Nucleation Values of Snomax, Kaolinite, and Montmorillonite

Compound	IN onset: this study (°C)	IN onset: literature values (°C)	Refs
Snomax	−4.8 ± 0.8	−2 to −6.6	47, 48, and 61
kaolinite	−11.8 ± 2.4	−10 to −14	50, 51, and 53
montmorillonite	−14.9 ± 0.6	−12 to −16.3	50, 52, and 53
illite NX	−15.5 ± 1.3	−11 °C to −27	25 and 70

The single particle ice nucleation onset temperatures of the particles produced from LPS, lipase, and lysozyme (Figure 5) have never been measured before. LPS, a bacterial degradation product, and lipase, an enzyme, are both marine relevant.[71,72] Lysozyme, a known bacterial enzyme found in marine aerosol, readily lyses peptidoglycan on the surface of Gram-positive bacteria.[73] The ice nucleation behavior of systems when acted

DOI: 10.1021/acs.analchem.9b01819
Anal. Chem. 2019, 91, 11138−11145

upon by lysozyme has been previously studied,[60,74] but the ice nucleation of lysozyme itself has not. In this study, we found all three systems to nucleate at −23.6 ± 0.7, −23.8 ± 1.1, and −25.2 ± 1.3 °C for LPS, lipase, and lysozyme, respectively, all which fall within the ice nucleation temperature range close to that of Milli-Q ultrapure water, indicating that they are not as good at nucleating ice as the minerals studied or as Snomax. It is not surprising that LPS is a poor INP due to its high relative abundance and the relatively low INP emissions from SSA.[32]

The ice nucleation behavior of Snomax was also probed after reaction with ozone. First, the reaction of ozone and oleic acid particles was measured as validation that ozone was reaching the environmental cell. The associated spectra of the reaction with ozone and oleic acid are shown in Supporting Information, Figure S5, showing that ozone was indeed reaching the substrate.

Spectra of Snomax before and after reaction, Figure 6, show a loss of peaks at 1125, 1350, 1550, and 1650 cm^{-1}, indicating

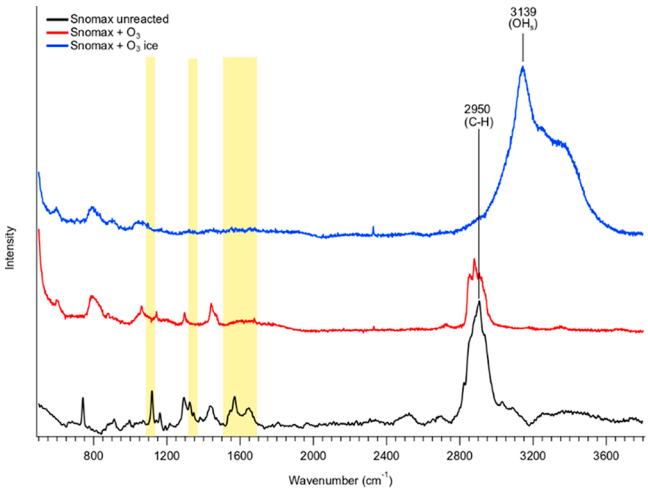

Figure 6. Raman spectra of Snomax, before (black) and after (red) reaction with ozone (O_3) and after ice nucleation (blue). Yellow highlighted regions correspond to peaks that have largely disappeared from the spectrum following exposure of Snomax to ozone.

a reaction occurred, but due to the fact that Snomax is a commercial product, we do not have access to its structure. The ice nucleation temperature is depressed following reaction with ozone, shifting from −4.8 ± 1.0 °C to −6.0 ± 1.3 °C. This is a statistically insignificant change in the onset temperature from the Snomax ice nucleation temperature before reaction with ozone, which agrees with findings from Attard et al.[48] What is most interesting is that although there are significant changes in the Snomax Raman spectrum following ozone exposure, there is only a slight change in the freezing behavior of Snomax, indicating that active sites for ice nucleation remain unchanged. This demonstrates the capabilities of this system to monitor the effect reactive gases have on ice nucleation behavior as well as changes in chemical composition and phase.

CONCLUSIONS

Herein we have characterized individual atmospherically relevant particles for their ice nucleation activity using an environmental cell that allows for spectroscopic and optical probing to the freezing process. The impact of exposure of ozone on ice nucleation activity of Snomax was also explored. It was shown that, although clear spectroscopic changes of the Raman spectrum of the Snomax particle occurred, there was only a small change in the ice nucleation activity. Future experiments will focus on identifying good INPs within the population of SSA particles collected from field studies to resolve ice nucleation behavior and mechanisms at the single particle level. Additionally, we are interested in determining the impact of heterogeneous chemistry and particle aging on ice nucleation for a wide range of particle types.

ASSOCIATED CONTENT

Supporting Information

The Supporting Information is available free of charge on the ACS Publications website at DOI: 10.1021/acs.analchem.9b01819.

Additional details of the experimental methods, relative humidity and temperature calibration data, and additional Raman spectra including heterogeneous reaction of ozone with oleic acid; Overall, five additional figures are included (PDF)

AUTHOR INFORMATION

Corresponding Author

*E-mail: vhgrassian@ucsd.edu.

ORCID

Vicki H. Grassian: 0000-0001-5052-0045

Notes

The authors declare no competing financial interest.

ACKNOWLEDGMENTS

The authors gratefully acknowledge the support of the National Science Foundation through the Center for Aerosol Impacts on the Chemistry of the Environment (CAICE), a Center for Chemical Innovation (CHE-1801971), and the National Science Foundation Graduate Research Fellowship Program (DGE-1650112). The authors also thank CAICE collaborators, including Dr. Paul DeMott, Dr. Tom Hill, Professor Kimberly Prather, Dr. Jonathan Trueblood, and Charlotte Dewald. The contents in this study do not necessarily reflect the official views of the National Science Foundation. The NSF does not endorse the purchase of the commercial products used in this report.

REFERENCES

(1) Lohmann, U.; Feichter, J. *Atmos. Chem. Phys. Discuss.* **2004**, *4* (6), 7561−7614.

(2) DeMott, P. J.; Mason, R. H.; McCluskey, C. S.; Hill, T. C. J.; Perkins, R. J.; Desyaterik, Y.; Bertram, A. K.; Trueblood, J. V.; Grassian, V. H.; Qiu, Y.; Molinero, V.; Tobo, Y.; Sultana, C. M.; Lee, C.; Prather, K. A. *Environ. Sci. Process. Impacts* **2018**, *20* (11), 1559−1569.

(3) Meyer, R. K. P. Contribution of Working Groups I, II and III to the Fifth Assessment Report of the Intergovernmental Panel on Climate Change. *Climate Change 2014: Synthesis Report*; PCC, Geneva, Switzerland, 2014; pp 1−151.

(4) Lau, K. M.; Wu, H. T. *Geophys. Res. Lett.* **2003**, *30* (24), 2−6.

(5) Rogers, D. C.; DeMott, P. J.; Borys, R.; Prenni, A. J.; Kreidenweis, S. M.; Murphy, D. M.; Thomson, D. S.; Cziczo, D. J. *Proc. Natl. Acad. Sci. U. S. A.* **2003**, *100* (25), 14655−14660.

(6) Murray, B. J.; O'sullivan, D.; Atkinson, J. D.; Webb, M. E. *Chem. Soc. Rev.* **2012**, *41*, 6519−6554.

DOI: 10.1021/acs.analchem.9b01819
Anal. Chem. 2019, 91, 11138−11145

(7) Intergovernamental Panel on Climate Change: Climate Change, 2013; http://www.climatechange2013.org/images/report/WG1AR5_Frontmatter_FINAL.pdf.
(8) Wang, B.; Knopf, D. A. *J. Geophys. Res.* **2011**, *116* (D3), 1−14.
(9) Cantrell, W.; Heymsfield, A. *Bull. Am. Meteorol. Soc.* **2005**, *86* (6), 795−807.
(10) Vali, G.; DeMott, P. J.; Möhler, O.; Whale, T. F. *Atmos. Chem. Phys.* **2015**, *15* (18), 10263−10270.
(11) Hiranuma, N.; Möhler, O.; Bingemer, H.; Bundke, U.; Cziczo, D. J.; Danielczok, A.; Ebert, M.; Garimella, S.; Hoffmann, N.; Höhler, K. K; Kanji, Z. A.; Kiselev, A.; Raddatz, M.; Stetzer, O. *AIP Conf. Proc.* **2013**, *1527*, 914−917.
(12) Wang, X.; Sultana, C. M.; Trueblood, J.; Hill, T. C. J.; Malfatti, F.; Lee, C.; Laskina, O.; Moore, K. A.; Beall, C. M.; McCluskey, C. S.; Cornwell, G. C.; Zhou, Y.; Cox, J. L.; Pendergra, K. A.; et al. *ACS Cent. Sci.* **2015**, *1* (3), 124−131.
(13) Hoose, C.; Möhler, O. *Atmos. Chem. Phys.* **2012**, *12*, 9817−9854.
(14) Pruppacher, H. R.; Klett, J. D. *Microphysics of Clouds and Precipitation*; Springer, 2010; Vol. *18*.
(15) Vali, G. *Bull. Am. Meteorol. Soc.* **1985**, *66*, 1426.
(16) Wise, M. E.; Baustian, K. J.; Koop, T.; Freedman, M. A.; Jensen, E. J.; Tolbert, M. A. *Atmos. Chem. Phys.* **2012**, *12* (2), 1121−1134.
(17) Knopf, D. A.; Koop, T. *J. Geophys. Res.* **2006**, *111* (12), 1−10.
(18) Kanji, Z. A.; Abbatt, J. P. D *J. Geophys. Res.* **2006**, *111* (16), 1−10.
(19) Primm, K. M.; Schill, G. P.; Veghte, D. P.; Freedman, M. A.; Tolbert, M. A. *J. Atmos. Chem.* **2017**, *74* (1), 55−69.
(20) Dymarska, M.; Murray, B. J.; Sun, L.; Eastwood, M. L.; Knopf, D. A.; Bertram, A. K. *J. Geophys. Res.* **2006**, *111* (D4), 1−9.
(21) Kanji, Z. A.; Ladino, L. A.; Wex, H.; Boose, Y.; Burkert-Kohn, M.; Cziczo, D. J.; Kramer, M. *Meteorol. Monogr.* **2017**, *58* (1), 1.1−1.33.
(22) Ansmann, A.; Tesche, M.; Althausen, D.; Müller, D.; Seifert, P.; Freudenthaler, V.; Heese, B.; Wiegner, M.; Pisani, G.; Knippertz, P.; Dubovik, O. *J. Geophys. Res.* **2008**, *113* (D4), 1−16.
(23) De Boer, G.; Morrison, H.; Shupe, M. D.; Hildner, R. *Geophys. Res. Lett.* **2011**, *38* (1), 1−5.
(24) Westbrook, C. D.; Illingworth, A. J. *Q. J. R. Meteorol. Soc.* **2013**, *139* (677), 2209−2221.
(25) Welti, A.; Kandler, K.; Petters, M. D.; Weinbruch, S.; Leisner, T.; Hader, J. D.; Boose, Y.; Dreischmeier, K.; Rose, D.; Tajiri, T.; Nillius, B.; Wright, T. P.; Kulkarni, G.; Augustin-Bauditz, S.; Saito, A.; Mohler, O.; Whale, T.; Kiselev, A.; Curtius, J.; Wex, H.; Peckhaus, A.; Schill, G. P.; Frank, F.; Hoffmann, N.; Hill, T. C. J.; Murray, B. J.; Tolbert, M. A.; Levin, E. J. T.; Murakami, M.; Kanji, Z. A.; Yamashita, K.; Danielczok, A.; Koop, T.; Hiranuma, N.; Sullivan, D.; Budke, C.; Niedermeier, D.; McCluskey, C. S.; Bingemer, H.; Ebert, M.; Diehl, K.; Demott, P. J. *Atmos. Chem. Phys.* **2015**, *15* (5), 2489−2518.
(26) Schill, G. P.; Tolbert, M. A. *J. Phys. Chem. C* **2014**, *118* (50), 29234−29241.
(27) Brooks, S. D.; Suter, K.; Olivarez, L. *J. Phys. Chem. A* **2014**, *118* (43), 10036−10047.
(28) Collier, K. N.; Brooks, S. D. *J. Phys. Chem. A* **2016**, *120*, 10169.
(29) Wang, B.; Knopf, D. A.; China, S.; Arey, B. W.; Harder, T. H.; Gilles, M. K.; Laskin, A. *Phys. Chem. Chem. Phys.* **2016**, *18* (43), 29721−29731.
(30) Phillips, V. T. J.; Donner, L. J.; Garner, S. T. *J. Atmos. Sci.* **2007**, *64* (3), 738−761.
(31) Meyers, M. P.; DeMott, P. J.; Cotton, W. R. *Journal of Applied Meteorology.* **1992**, *31*, 708−721.
(32) McCluskey, C. S.; Hill, T. C. J.; Sultana, C. M.; Laskina, O.; Trueblood, J.; Santander, M. V.; Beall, C. M.; Michaud, J. M.; Kreidenweis, S. M.; Prather, K. A.; Grassian, V. H.; DeMott, P. J. *J. Atmos. Sci.* **2018**, *75* (7), 2405−2423.
(33) Wise, M. E.; Baustian, K. J.; Tolbert, M. A. *Proc. Natl. Acad. Sci. U. S. A.* **2010**, *107* (15), 6693−6698.
(34) Schill, G. P.; Tolbert, M. A. *J. Phys. Chem. C* **2014**, *118* (50), 29234−29241.
(35) Wilson, T. W.; Ladino, L. A.; Alpert, P. A.; Breckels, M. N.; Brooks, I. M.; Browse, J.; Burrows, S. M.; Carslaw, K. S.; Huffman, J. A.; Judd, C.; Kilthau, W. P.; Mason, R. H.; McFiggans, G.; Miller, L. A.; Najera, J. J.; Polishchuk, E.; Rae, S.; Schiller, C. L.; Si, M.; Temprado, J. V.; Whale, T. F.; Wong, J. P. S.; Wurl, O.; Yakobi-Hancock, J. D.; Abbatt, J. P. D; Aller, J. Y.; Bertram, A. K.; Knopf, D. A.; Murray, B. J. A *Nature* **2015**, *525* (7568), 234−238.
(36) Schill, G. P.; Genareau, K.; Tolbert, M. A. *Atmos. Chem. Phys.* **2015**, *15*, 7523−7536.
(37) Knopf, D. A.; Luo, B. P.; Krieger, U. K.; Koop, T. *J. Phys. Chem. A* **2003**, *107*, 4322−4322.
(38) Knopf, D. A.; Koop, T.; Luo, B. P.; Weers, U. G.; Peter, T. *Atmos. Chem. Phys.* **2002**, *2* (3), 207−214.
(39) Murphy, D. M.; Koop, T. *Q. J. R. Meteorol. Soc.* **2005**, *131* (608), 1539−1565.
(40) Laskina, O.; Morris, H. S.; Grandquist, J. R.; Qin, Z.; Stone, E. A.; Tivanski, A. V.; Grassian, V. H. *J. Phys. Chem. A* **2015**, *119* (19), 4489−4497.
(41) Lu, P. D.; Wang, F.; Zhao, L. J.; Li, W. X.; Li, X. H.; Dong, J. L.; Zhang, Y. H.; Lu, G. Q. *J. Chem. Phys.* **2008**, *129* (10), 1−8.
(42) Estillore, A. D.; Morris, H. S.; Or, V. W.; Lee, H. D.; Alves, M. R.; Marciano, M. A.; Laskina, O.; Qin, Z.; Tivanski, A. V.; Grassian, V. H. *Phys. Chem. Chem. Phys.* **2017**, *19* (31), 21101−21111.
(43) Zhang, Y. H.; Chan, C. K. *J. Phys. Chem. A* **2002**, *106* (2), 285−292.
(44) Baustian, K. J.; Wise, M. E.; Tolbert, M. A. *Atmos. Chem. Phys.* **2010**, *10*, 2307−2317.
(45) Martin, S. T. *Chem. Rev.* **2000**, *100* (9), 3403−3453.
(46) Buck, A. L. *J. Appl. Meteorol.* **1981**, *20* (12), 1527−1532.
(47) Hartmann, S.; Augustin, S.; Clauss, T.; Voigtländer, J.; Niedermeier, D.; Wex, H.; Stratmann, F. *Atmos. Chem. Phys. Discuss.* **2012**, *12* (8), 21321−21353.
(48) Attard, E.; Yang, H.; Delort, A. M.; Amato, P.; Pöschl, U.; Glaux, C.; Koop, T.; Morris, C. E. *Atmos. Chem. Phys.* **2012**, *12* (22), 10667−10677.
(49) O'Sullivan, D.; Murray, B. J.; Ross, J. F.; Webb, M. E. *Atmos. Chem. Phys.* **2016**, *16* (12), 7879−7887.
(50) Mortazavi, R.; Hayes, C. T.; Ariya, P. A. *Environ. Chem.* **2008**, *5* (6), 373−381.
(51) Zimmermann, F.; Weinbruch, S.; Schütz, L.; Hofmann, H.; Ebert, M.; Kandler, K.; Worringen, A. *J. Geophys. Res.* **2008**, *113* (23), 113.
(52) Pitter, R. L.; Pruppacher, H. R. *Q. J. R. Meteorol. Soc.* **1973**, *99*, 540−550.
(53) Diehl, K.; Simmel, M.; Wurzler, S. *Atmos. Environ.* **2007**, *41* (2), 303.
(54) Orser, C. S.; Staskawicz, J. B.; Panopoulos, N. J.; Dahlbeck, D.; Lindow, S. E. *Phytopathology* **1982**, *72* (7), 1000.
(55) Gurian-Sherman, D.; Lindow, S. E. Bacterial Ice Nucleation: Significance and Molecular Basis. *FASEB J.* **1993**.71338
(56) Pummer, B. G.; Bauer, H.; Bernardi, J.; Bleicher, S.; Grothe, H. *Atmos. Chem. Phys.* **2012**, *12* (5), 2541−2550.
(57) Kanji, Z. A.; DeMott, P. J.; Mohler, O.; Abbatt, J. P. D. *Atmos. Chem. Phys.* **2011**, *11* (1), 31−41.
(58) Koop, T.; Zobrist, B. *Phys. Chem. Chem. Phys.* **2009**, *11* (46), 10839−10850.
(59) Wood, S. E.; Baker, M. B.; Swanson, B. D. *Rev. Sci. Instrum.* **2002**, *73* (11), 3988−3996.
(60) Pandey, R.; Usui, K.; Livingstone, R. A.; Fischer, S. A.; Pfaendtner, J.; Backus, E. H. G.; Nagata, Y.; Fro hlich-Nowoisky, J.; Schmu ser, L.; Mauri, S.; Scheel, J. F.; Knopf, D. A.; Po schl, U.; Bonn, M.; Weidner, T. *Sci. Adv.* **2016**, *2* (4), 1−8.
(61) Polen, M.; Lawlis, E.; Sullivan, R. C. *Journal of Geophysical Research: Atmospheres Bacterial Particles* **2016**, *121* (19), 666−678.
(62) Kanji, Z. A.; Lohmann, U.; Welti, A.; Stetzer, O.; Lüönd, F. *J. Atmos. Sci.* **2014**, *71* (1), 16−36.
(63) Murray, B. J.; Broadley, S. L.; Wilson, T. W.; Atkinson, J. D.; Wills, R. H. *Atmos. Chem. Phys.* **2011**, *11* (9), 4191−4207.

DOI: 10.1021/acs.analchem.9b01819
Anal. Chem. 2019, 91, 11138−11145

(64) Wheeler, M. J.; Bertram, A. K. *Atmos. Chem. Phys.* **2012**, *12*, 1189−1201.
(65) Alpert, P. A.; Knopf, D. A. *Atmos. Chem. Phys.* **2016**, *16* (4), 2083−2107.
(66) Knopf, D. A.; Alpert, P. A.; Wang, B. *ACS Earth Sp. Chem.* **2018**, *2* (3), 168−202.
(67) Tobo, Y.; Demott, P. J.; Hill, T. C. J.; Prenni, A. J.; Swoboda-Colberg, N. G.; Franc, G. D.; Kreidenweis, S. M. *Atmos. Chem. Phys.* **2014**, *14* (16), 8521−8531.
(68) Beall, C. M.; Stokes, M. D.; Hill, T. C.; Demott, P. J.; Dewald, J. T.; Prather, K. A. *Atmos. Meas. Tech.* **2017**, *10*, 2613−2626.
(69) Whale, T. F.; Murray, B. J.; Wilson, T. W.; Umo, N. S.; Baustian, K. J.; Atkinson, J. D.; Workneh, D. A.; Morris, G. J. *Atmos. Meas. Tech.* **2015**, *8*, 2437−2447.
(70) Broadley, S. L.; Murray, B. J.; Herbert, R. J.; Atkinson, J. D.; Dobbie, S.; Malkin, T. L.; Condliffe, E.; Neve, L. *Atmos. Chem. Phys.* **2012**, *12*, 287−307.
(71) Cochran, R. E.; Laskina, O.; Trueblood, J. V.; Estillore, A. D.; Morris, H. S.; Jayarathne, T.; Sultana, C. M.; Lee, C.; Lin, P.; Laskin, J.; Laskin, A.; Dowling, J. A.; Qin, Z.; Cappa, C. D.; Bertram, T. H.; Tivanski, A. V.; Stone, E. A.; Prather, K. A.; Grassian, V. H. *Chem* **2017**, *2* (5), 655−667.
(72) Schiffer, J. M.; Luo, M.; Dommer, A. C.; Thoron, G.; Pendergraft, M.; Santander, M. V.; Lucero, D.; Pecora De Barros, E.; Prather, K. A.; Grassian, V. H.; Amaro, R. E. *J. Phys. Chem. Lett.* **2018**, *9* (14), 3839−3849.
(73) Michaud, J. M.; Thompson, L. R.; Kaul, D.; Espinoza, J. L.; Richter, R. A.; Xu, Z. Z.; Lee, C.; Pham, K. M.; Beall, C. M.; Malfatti, F.; Azam, F.; Knight, R.; Burkart, M. D.; Dupont, C. L.; Prather, K. A. *Nat. Commun.* **2018**, *9*, na.
(74) Hill, T. C. J.; Demott, P. J.; Tobo, Y.; Fröhlich-Nowoisky, J.; Moffett, B. F.; Franc, G. D.; Kreidenweis, S. M. *Atmos. Chem. Phys.* **2016**, *16* (11), 7195−7211.

DOI: 10.1021/acs.analchem.9b01819
Anal. Chem. 2019, 91, 11138−11145